INTERNATIONAL JOURNAL OF
NUMERICAL ANALYSIS AND MODELING
Volume 22, Number 2, Pages 226–245

doi: 10.4208/ijnam2025-1011

NUMERICAL STUDIES FOR AN INTERFACE PROBLEM INVOLVING FOURTH- AND SECOND-ORDER POISSON-FERMI ELECTROSTATIC EQUATIONS

MENGJIE LIU, MINGYAN HE, AND PENGTAO SUN

Abstract. A class of particular interface problems, which is derived from Bazant-Storey-Kornyshev (BSK) theory to account for the electrostatic correlation in concentrated electrolytes, is studied in this paper. It involves a modified fourth-order Poisson-Fermi equation in solvents and a second-order Poisson equation in solutes with high-contrast coefficients, where nonhomogeneous interface conditions are introduced over the interface that divides solutes from solvents. A type of interface-fitted finite element method is developed and analyzed for this interface problem, and optimal error estimates are obtained for all variables in both H^1 and L^2 norms. Numerical experiments validate all attained theoretical results through two mathematical examples, as well as the electrostatic correlation phenomenon in concentrated electrolytes through a physical example, practically, where the electrostatic stress and interactional forces in the concentrated electrolyte are computed to reveal the charge reversal phenomenon that is governed by the BSK theory.

Key words. Fourth-/second-order Poisson-Fermi interface problem, nonhomogeneous interface condition, interface-fitted finite element method, optimal convergence, electrostatic correlation, charge reversal.

1. Introduction

In biological processes and colloidal stabilities, electrostatic interactions between the charged objects in solution and their ionic atmospheres play an important role [1], such as the biological activity of proteins [2, 3, 4], the self-assembly of biomolecules [5, 6] and the ions' adsorption on lipid membranes [7, 8, 9]. The study of electrostatic interactions can have a better understanding on the molecular function in cells and improve the efficacy of biomedical drugs. The Poisson-Boltzmann (PB) continuum model that is based on the mean-field approximation has been used to simulate the distribution of ions around charged surfaces for nearly a century [10], where the ions are treated as point charges which only interact with the background electric potential arising from the charges in the system. So the ionic steric effect and electrostatic interactions between ions have been ignored. However, such ignored effects are crucial to describe the ion transport in some situations, such as the charge dynamics in concentrated electrolytes and ions permeation through ion channels. To overcome the limitations, many efforts have been made to improve the PB continuum model in order to correctly describe the spatial and related effects in electrolytes and ionic liquids [11, 12, 10, 13].

Recently, based on the Santangelo's work [14], Bazant, Storey, and Kornyshev propose a modified PB model to depict the electrostatic potential field (e.g., the solvent region Ω_1 in Fig. 1) by substituting the following fourth-order Poisson-Fermi equation for the classical second-order PB equation under the consideration

Received by the editors on April 10, 2024 and, accepted on October 16, 2024.
2000 *Mathematics Subject Classification.* 65N30, 35G30, 35R05, 35Q35.

of electrostatic correlation effects [15, 16],

$$\epsilon_1(l_c^2\Delta^2\phi_1 - \Delta\phi_1) = \rho(\phi_1), \quad \boldsymbol{x} \in \Omega_1, \tag{1}$$

where ϕ_1 is the electrostatic potential defined in the solvent surrounding the solute (molecule), ϵ_1 is the dielectric constant of electrolyte, and l_c is the electrostatic length. The above new theory is therefore called BSK theory, which can be turned back to the classical PB theory by letting $l_c = 0$ in (1), leading to the following second-order Poisson-type electrostatic potential equation defined in either solvents or solutes (e.g., the solute region Ω_2 in Fig. 1):

$$-\epsilon_2\Delta\phi_2 = 0, \quad \boldsymbol{x} \in \Omega_2, \tag{2}$$

where ϕ_2 and ε_2 are the electrostatic potential and dielectric permittivity, respectively, in the solute. Both ϵ_1 and ϵ_2 are positive. The Fermi-like charge density distribution in (1), $\rho(\phi_1)$, is defined as [15, 17, 10]:

$$\rho(\phi_1) = z_1 e C_1 + z_2 e C_2,$$

where C_1 and C_2 represent ion species concentrations in solvent, defined as [16]:

$$\left\{ \begin{array}{l} C_1 = C_\infty^+ e^{-z_1 \frac{e}{K_B T}\phi_1}, \\ C_2 = C_\infty^- e^{-z_2 \frac{e}{K_B T}\phi_1}, \end{array} \right. \tag{3}$$

where e is the unit charge, K_B the Boltzmann constant and T the absolute temperature, C_∞^+ and C_∞^- indicate the far field concentrations of cations and anions in electrolytes, respectively, z_1 (resp., z_2) is the valence of cations (resp., anions) with the opposite sign (such as $z_1 = 3, z_2 = -1$), satisfying $z_1 C_\infty^+ = z_2 C_\infty^-$. Then,

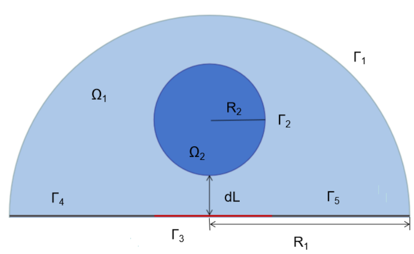

FIGURE 1. The geometry of a solvation system with an implicit solvent, where the solvent-solute interface Γ_2 separates the solvent region Ω_1 and the molecular (solute) region Ω_2. The red segment, Γ_3, represents a charged plate.

the following boundary conditions and interface conditions are proposed for the above interface problem involving the fourth-order Poisson-Fermi equation (1) and second-order Poisson equation (2) on either side of the interface,

$$\left\{ \begin{array}{ll} \phi_1 = \phi_2, & \text{on } \Gamma_2, \\ \epsilon_1 \frac{\partial\phi_1}{\partial \boldsymbol{n}_1} + \epsilon_2 \frac{\partial\phi_1}{\partial \boldsymbol{n}_2} = -\sigma, & \text{on } \Gamma_2, \\ \phi_1 = 0, & \text{on } \Gamma_1, \\ \epsilon_1 \frac{\partial\phi_1}{\partial \boldsymbol{n}_1} = \left\{ \begin{array}{ll} \sigma, & \text{on } \Gamma_3, \\ 0, & \text{on } \Gamma_4, \Gamma_5, \end{array} \right. & \\ -\Delta\phi_1 = g, & \text{on } \partial\Omega_1, \end{array} \right. \tag{4}$$

where $\boldsymbol{n}_1$ (resp., $\boldsymbol{n}_2$) denotes the outward normal unit vector pointing to the outside of Ω_1 (resp., Ω_2), g is a known function given by experimental or hypothetical data, σ represents the charge on the surface of ion or charged plate, which makes Neumann-type interface- and boundary conditions nonhomogeneous on Γ_2 and Γ_3 (i.e., (4)$_2$ and (4)$_4$), respectively, and $\partial\Omega_1 = \bigcup_{i=1}^{5} \Gamma_i$. Fig. 1 illustrates a schematic domain in which the particular interface problem is defined, here Γ_2 denotes the interface between the solvent (e.g., the electrolyte) and solute (e.g., the charged ion) on which two interface conditions (4)$_1$ and (4)$_2$ are introduced, and, Γ_3 represents a charged plate whose charge is opposite to the charge of ion/particle, as shown in (4)$_2$ and (4)$_4$ where σ owns opposite signs on Γ_2 and Γ_3. Note that besides (4)$_1$-(4)$_4$, one more nonhomogeneous boundary condition on $\partial\Omega_1$, (4)$_5$, is introduced to ensure the well-posedness of fourth-order Poisson-Fermi equation that is defined in Ω_1.

Since the geometric size of charged particles is measured in nanometers, to avoid possible rounding errors arising from the usage of SI as the unit of length, we non-dimensionalize the above interface problem through the scales $\hat{x} = \frac{x}{\lambda_D}$, $\hat{\phi}_i = \frac{e}{K_B T}\phi_i$ $(i = 1, 2)$ and $\delta_c = \frac{l_c}{\lambda_D}$, where the Debye length λ_D can be defined as follows [18],

$$\lambda_D = \sqrt{\frac{\epsilon_1 K_B T}{e^2 C_\infty^+ z_1(z_1 - z_2)}}. \tag{5}$$

Therefore, the following dimensionless interface problem is defined, accordingly,

$$\begin{cases} \delta_c^2 \Delta^2 \hat{\phi}_1 - \Delta\hat{\phi}_1 = \frac{e^{-z_1\hat{\phi}_1} - e^{-z_2\hat{\phi}_1}}{z_1 - z_2}, & \text{in } \Omega_1, \\ -\epsilon_r \Delta\hat{\phi}_2 = 0, & \text{in } \Omega_2, \\ \hat{\phi}_1 = \hat{\phi}_2, & \text{on } \Gamma_2, \\ \frac{\partial\hat{\phi}_1}{\partial\hat{\boldsymbol{n}}_1} + \varepsilon_r \frac{\partial\hat{\phi}_2}{\partial\hat{\boldsymbol{n}}_2} = -\frac{e\lambda_D}{K_B T\epsilon_1}\sigma, & \text{on } \Gamma_2, \\ \hat{\phi}_1 = 0, & \text{on } \Gamma_1, \\ \frac{\partial\hat{\phi}_1}{\partial\hat{\boldsymbol{n}}_1} = \begin{cases} \frac{e\lambda_D}{K_B T\epsilon_1}\sigma, & \text{on } \Gamma_3, \\ 0, & \text{on } \Gamma_4, \Gamma_5, \end{cases} & \\ -\Delta\hat{\phi}_1 = \hat{g}, & \text{on } \partial\Omega_1, \end{cases} \tag{6}$$

where $\epsilon_r = \frac{\epsilon_2}{\epsilon_1}$, $\hat{g} = \frac{e\lambda_D^2}{K_B T} g$.

Interface problems arise in many applications of fluid mechanics and materials science, where their governing partial differential equations (PDEs) have discontinuous and even high-contrast coefficients across interfaces, making corresponding numerical methodologies and computations challenging. The construction of numerical solutions for interface problems can be traced back to the 1970s, and has become a subject of in-depth study since then [19, 20, 21, 22]. Some important progresses include but not limited to the following works: an immersed interface finite difference method for elliptic interface problems is proposed in [23], where the uniformly triangulated mesh unfits the interface in a regular domain; The second order elliptic and parabolic interface problems are solved and analyzed by finite element method in [24], where the interface is allowed to be of arbitrary shape and smooth; Both interface-fitted arbitrary Lagrangian-Eulerian finite element methods and interface-unfitted fictitious domain finite element methods are developed and/or analyzed by the author Sun et al. in [25, 26, 27, 28, 29, 30, 31, 32, 33, 34] for parabolic/parabolic-, Stokes/Stokes-, Stokes/elliptic-, Stokes/parabolic moving interface problems as well as realistic fluid-structure interaction problems, and etc. The standard and mixed FEMs were studied by the author He et al. [35] for a modified fourth-order Poisson-Fermi equation in a single domain, only. To the best of our knowledge, few attempts have been made so far on numerically solving the fourth-/second-order nonlinear Poisson-Fermi interface problem. In this paper, we first adopt the splitting method to split the fourth-order Poisson-Fermi equation into two coupled second order Poisson-like equations, while interacting with the second-order Poisson equation on the other side of the interface through interface conditions. Then correspondingly, we develop a type of interface-fitted finite element method to discretize the above interface problem, and conduct the finite element error analysis concluded with optimal error estimates in both H^1 and L^2 norms. In addition, we also study finite element approximations to the electrostatic stress and then to the interaction forces in the concentrated electrolyte, for the sake of investigating the charge reversal process. Finally, numerical experiments are carried out to validate all theoretical convergence results through two self-defined mathematical interface problems, then to validate the BSK theory-induced charge reversal phenomenon via a physical electrostatic correlation problem, practically.

The structure of this paper is organized as follows. In Section 2, we propose the finite element discretization for the presented interface problem and analyze its optimal convergence properties. Numerical experiments and validations are carried out in Section 3, where a physical example is presented to account for the electrostatic correlation as well. Lastly, the concluding remarks are given in Section 4.

Some symbols are introduced below that will be used throughout the rest of this paper. For each integer $m \geq 0$ and real p with $1 \leq p \leq \infty$, $W^{m,p}(\Omega)$ denotes the standard Sobolev space of real functions with their weak derivatives of order up to m in the Lebesgue space $L^p(\Omega)$. When $p = 2$, $W^{m,2}(\Omega)$ is simplified as $H^m(\Omega)$, and $H^0(\Omega)$ coincides with $L^2(\Omega)$ when $m = 0$. The standard L^2 inner product over a domain Ω or a boundary Γ is denoted as $(u, \tilde{u}) = \int_\Omega u\tilde{u}dx$ and $< u, \tilde{u} >_\Gamma = \int_\Gamma u\tilde{u}ds$, respectively. In what follows, C is generally used to represent a generic constant that is irrelevant with any discretization parameter such as the mesh size h.

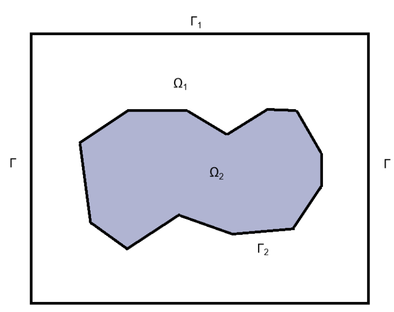

FIGURE 2. The computational domain Ω that is formed by subdomains Ω_1, Ω_2 and interface Γ_2.

2. Modeling and numerical methodology

2.1. Model generalization and weak form. Let Ω be a convex polygon or polyhedron in $\mathbb{R}^d$ ($d=2,3$), and $\Omega := \Omega_1 \cup \Omega_2$, where both Ω_1 and Ω_2 are polygon or polyhedron, representing the subdomains of solvent and solute, respectively. The interface $\Gamma_2 = \partial\Omega_1 \cap \partial\Omega_2$, and $\Gamma = \partial\Omega_1 \setminus (\Gamma_1 \cup \Gamma_2) = \Gamma_3 \cup \Gamma_4 \cup \Gamma_5$, as shown in Fig. 2. Without loss of generality, we rewrite (6) to the following a class of nonlinear fourth-order/second-order nonlinear Poisson-Fermi interface problem with jump coefficients by generalizing all right hand side/boundary value functions in (6) and removing all symbols " $\hat{\ }$ " from (6),

$$
\begin{cases}
\delta_c^2 \Delta^2 \phi_1 - \Delta\phi_1 = \rho(\phi_1) + f_1, & \text{in } \Omega_1,\\
-\epsilon_r \Delta\phi_2 = f_2, & \text{in } \Omega_2,\\
\frac{\partial\phi_1}{\partial \boldsymbol{n}_1} + \epsilon_r \frac{\partial\phi_2}{\partial \boldsymbol{n}_2} = g_2, & \text{on } \Gamma_2,\\
\phi_1 = \phi_2, & \text{on } \Gamma_2,\\
\phi_1 = g_1, & \text{on } \Gamma_1,\\
\frac{\partial\phi_1}{\partial \boldsymbol{n}_1} = g_3, & \text{on } \Gamma,\\
-\Delta\phi_1 = g, & \text{on } \partial\Omega_1,\\
\phi_2 = g_4, & \text{on } \partial\Omega_2 \setminus \Gamma_2,
\end{cases} \tag{7}
$$

where $f_i \in L^2(\Omega_i)$ $(i=1,2)$ denotes the extra linear source/sink term in each subdomain. The boundary condition $(7)_8$ only holds when Ω_2 is not immersed in Ω_1 and is attached to the outer boundary (e.g., the back-to-back case shown in Fig. 3).

By splitting the fourth-order Poisson-Fermi equation $(7)_1$ into two coupled second-order Poisson equations, we reformulate (7) to the following equivalent interface problem,

$$
\begin{cases}
-\Delta\phi_1 = u, & \text{in } \Omega_1,\\
-\epsilon_r \Delta\phi_2 = f_2, & \text{in } \Omega_2,\\
\phi_1 = g_1, & \text{on } \Gamma_1,\\
\frac{\partial\phi_1}{\partial \boldsymbol{n}_1} + \epsilon_r \frac{\partial\phi_2}{\partial \boldsymbol{n}_2} = g_2, & \text{on } \Gamma_2,\\
\phi_1 = \phi_2, & \text{on } \Gamma_2,\\
\frac{\partial\phi_1}{\partial \boldsymbol{n}_1} = g_3, & \text{on } \Gamma,\\
\phi_2 = g_4, & \text{on } \partial\Omega_2 \setminus \Gamma_2,
\end{cases} \tag{8}
$$

and,

$$
\begin{cases}
-\delta_c^2 \Delta u + u = \rho(\phi_1) + f_1, & \text{in } \Omega_1,\\
u = g, & \text{on } \partial\Omega_1.
\end{cases} \tag{9}
$$

The well-posedness of the system (8) and (9) can be naturally obtained by the well-posedness of fourth-order modified Poisson-Fermi equation [36], that is, there exists a unique solution, $\phi_1 \in H^4(\Omega_1) \subset L^2(\Omega_1)$, $\phi_2 \in H^2(\Omega_2) \subset L^2(\Omega_2)$, satisfying (7), where the interface condition $(7)_3$ is treated as Neumann boundary condition of $(7)_1$, and the other interface condition $(7)_4$ is taken as Dirichlet boundary condition of $(7)_2$, respectively, in a partitioned fashion.

Introduce the following notations of Sobolev spaces:

$$
\begin{aligned}
&\boldsymbol{Q} := \{(w_1, w_2) \in H^1(\Omega_1) \times H^1(\Omega_2) : w_1|_{\Gamma_1} = g_1, w_2|_{\partial\Omega_2\setminus\Gamma_2} = g_4, w_1|_{\Gamma_2} = w_2|_{\Gamma_2}\},\\
&\boldsymbol{Q^0} := \{(w_1, w_2) \in H^1(\Omega_1) \times H^1(\Omega_2) : w_1|_{\Gamma_1} = 0, w_2|_{\partial\Omega_2\setminus\Gamma_2} = 0, w_1|_{\Gamma_2} = w_2|_{\Gamma_2}\},\\
&W := \{u \in H^1(\Omega_1) : u|_{\partial\Omega_1} = g\}.
\end{aligned}
$$

Then, we can define the coupled weak form of (8) and (9) as follows: find $(\phi_1,\phi_2)\in \boldsymbol{Q}$ and $u\in W$ such that

$$(10)\quad \begin{cases} (\nabla\phi_1,\nabla\tilde{\phi}_1)_{\Omega_1}+\epsilon_r(\nabla\phi_2,\nabla\tilde{\phi}_2)_{\Omega_2}=(u,\tilde{\phi}_1)_{\Omega_1}+<g_2,\tilde{\phi}_1>_{\Gamma_2} \\ \qquad\qquad +<g_3,\tilde{\phi}_1>_{\Gamma}+(f_2,\tilde{\phi}_2)_{\Omega_2},\ \forall(\tilde{\phi}_1,\tilde{\phi}_2)\in \boldsymbol{Q^0}, \\ \delta_c^2(\nabla u,\nabla\tilde{u})_{\Omega_1}+(u,\tilde{u})_{\Omega_1}=(\rho(\phi_1),\tilde{u})_{\Omega_1}+(f_1,\tilde{u})_{\Omega_1},\ \forall\tilde{u}\in H_0^1(\Omega_1). \end{cases}$$

2.2. Finite element approximation. Firstly, we triangulate Ω with a finite set of closed triangles $\mathcal{T}_h=\{K\}$ that conforms across the interface Γ_2, each $K\in\mathcal{T}_h$ lies in either Ω_1 or Ω_2, and has at most two vertices lying on Γ_2. Then we define the following finite element spaces:

$$\begin{aligned} &V_h^i:=\{v\in H^1(\Omega_i): v|_K\in P^k(K),\forall K\in\mathcal{T}_h\},\ i=1,2,\\ &\boldsymbol{Q_h}:=\{(v_1,v_2)\in V_h^1\times V_h^2: v_1|_{\Gamma_1}=\Pi_h g_1, v_2|_{\partial\Omega_2\backslash\Gamma_2}=\Pi_h g_4, v_1|_{\Gamma_2}=v_2|_{\Gamma_2}\},\\ &\boldsymbol{Q_h^0}:=\{(v_1,v_2)\in V_h^1\times V_h^2: v_1|_{\Gamma_1}=0, v_2|_{\partial\Omega_2\backslash\Gamma_2}=0, v_1|_{\Gamma_2}=v_2|_{\Gamma_2}\},\\ &W_h:=\{v\in V_h^1: v|_{\partial\Omega_1}=\Pi_h g\},\\ &W_h^0:=\{v\in V_h^1: v|_{\partial\Omega_1}=0\}, \end{aligned}$$

where $P^k(K)$ represents the k-th $(k\geq 1)$ degree piecewise linear polynomial defined in each element $K\in\mathcal{T}_h$, Π_h is the finite element interpolation operator associated with $V_h^1\times V_h^2$. Thus, we are able to define the following interface-fitted finite element approximation to the coupled weak form (10): find $(\phi_{1,h},\phi_{2,h})\in\boldsymbol{Q_h}$ and $u_h\in W_h$ such that

$$(11)\quad \begin{cases} (\nabla\phi_{1,h},\nabla\tilde{\phi}_1)_{\Omega_1}+\epsilon_r(\nabla\phi_{2,h},\nabla\tilde{\phi}_2)_{\Omega_2}=(u_h,\tilde{\phi}_1)_{\Omega_1}+<g_2,\tilde{\phi}_1>_{\Gamma_2} \\ \qquad\qquad +<g_3,\tilde{\phi}_1>_{\Gamma}+(f_2,\tilde{\phi}_2)_{\Omega_2},\forall(\tilde{\phi}_1,\tilde{\phi}_2)\in\boldsymbol{Q_h^0}, \\ \delta_c^2(\nabla u_h,\nabla\tilde{u})_{\Omega_1}+(u_h,\tilde{u})_{\Omega_1}=(\rho(\phi_{1,h}),\tilde{u})_{\Omega_1}+(f_1,\tilde{u})_{\Omega_1},\forall\tilde{u}\in W_h^0. \end{cases}$$

Due to its nonlinearity, (11) needs to be properly linearized first before a numerical implementation is possibly conducted. We adopt the Picard's linearization to iteratively solve (11), as shown in Algorithm 1.

Remark 2.1. *The well-posedness property of the finite element approximation (11) can be verified through its Picard's linearization process (12) and (13). First, due to the elliptic property of (12) in a single domain Ω_1, its well-posedness is obvious with the known $\phi_{1,h}^n$ obtained from the previous iteration step. Thereafter, by virtue of the obtained u_h^{n+1} from (12), (13) becomes a well defined elliptic interface problem whose well-posedness has been studied in* [24]*. Therefore, (11) is well-posed as long as an initial guess $\phi_{1,h}^0$ is given and the Picard's linearization iteration is a convergent process, which actually has been long verified for many general cases (e.g., see* [37, 38, 39, 40]*).*

2.3. Finite element error analysis. To obtain the error estimate of (11) in L^2-norm, we introduce the following lemmas first.

Lemma 2.1. [41] *Let $(\Pi_h\phi_1,\Pi_h\phi_2)\in\boldsymbol{Q_h^0}$ and $\Pi_h u\in W_h^0$ be the finite element interpolation of $(\phi_1,\phi_2)\in\boldsymbol{Q}$ and $u\in W$. Then there exists a constant C independent*

Algorithm 1 Nonlinear iteration of Picard's linearization for the solution of (11).

1. Initialization of the iteration: set n=0 and let $\phi_{1,h}^0$=0 be the initial guess.
2. At the $(n+1)$-th iteration step ($n = 0, 1, 2, \cdots$), find $(\phi_{1,h}^{n+1}, \phi_{2,h}^{n+1}) \in \boldsymbol{Q_h}$ and $u_h^{n+1} \in W_h$ such that

$$\delta_c^2(\nabla u_h^{n+1}, \nabla\tilde{u})_{\Omega_1} + (u_h^{n+1}, \tilde{u})_{\Omega_1} = (\rho(\phi_{1,h}^n), \tilde{u})_{\Omega_1} + (f_1, \tilde{u})_{\Omega_1}, \ \forall\tilde{u} \in W_h^0, \tag{12}$$

$$\begin{aligned}(\nabla\phi_{1,h}^{n+1}, \nabla\tilde{\phi}_1)_{\Omega_1} + \epsilon_r(\nabla\phi_{2,h}^{n+1}, \nabla\tilde{\phi}_2)_{\Omega_2} = (u_h^{n+1}, \tilde{\phi}_1)_{\Omega_1} + < g_2, \tilde{\phi}_1 >_{\Gamma_2} \\ + < g_3, \tilde{\phi}_1 >_{\Gamma} + (f_2, \tilde{\phi}_2)_{\Omega_2}, \ \forall(\tilde{\phi}_1, \tilde{\phi}_2) \in \boldsymbol{Q_h^0}.\end{aligned} \tag{13}$$

3. Check the stopping criterion for the iteration: for a given tolerance ς, stop the iteration if

$$\|\phi_{1,h}^{n+1} - \phi_{1,h}^n\| + \|u_h^{n+1} - u_h^n\| \le \varsigma, \tag{14}$$

   and let $(\phi_{1,h}, \phi_{2,h}, u_h) = (\phi_{1,h}^{n+1}, \phi_{2,h}^{n+1}, u_h^{n+1})$. Otherwise, set $n+1$ to n, go back to Step 2 and continue the iteration.

---

of h, such that

$$\begin{aligned}&\|\phi_1 - \Pi_h\phi_1\|_{L^2(\Omega_1)} + h\|\phi_1 - \Pi_h\phi_1\|_{H^1(\Omega_1)} \le Ch^{k+1}, \\ &\|\phi_2 - \Pi_h\phi_2\|_{L^2(\Omega_2)} + h\|\phi_2 - \Pi_h\phi_2\|_{H^1(\Omega_2)} \le Ch^{k+1}, \\ &\|u - \Pi_h u\|_{L^2(\Omega_2)} + h\|u - \Pi_h u\|_{H^1(\Omega_2)} \le Ch^{k+1}.\end{aligned}$$

Lemma 2.2. *Let $(\phi_{1,h}, \phi_{2,h}, u_h)$ be the solution of (11) . Then for a sufficiently small h, we have*

$$\begin{aligned}&\|\phi_1 - \phi_{1,h}\|_{L^2(\Omega_1)} + \|\phi_2 - \phi_{2,h}\|_{L^2(\Omega_2)} \\ \le& C\left(h^2\|u - u_h\|_{L^2(\Omega_1)} + h^3\|\nabla(u - u_h)\|_{L^2(\Omega_1)}\right. \\ &\left. + h\|\nabla(\phi_1 - \phi_{1,h})\|_{L^2(\Omega_1)} + h\|\nabla(\phi_2 - \phi_{2,h})\|_{L^2(\Omega_2)} + \|\phi_1 - \phi_{1,h}\|_{L^2(\Omega_1)}^2\right).\end{aligned} \tag{15}$$

Proof. First, we define the following adjoint problem of (7): find $w_1 \in H^4(\Omega_1)$ and $w_2 \in H^2(\Omega_2)$ such that

$$\begin{cases} \delta_c^2\Delta^2 w_1 - \Delta w_1 - \rho'(\phi_1)w_1 = \xi_1, & \text{in } \Omega_1, \\ -\epsilon_r\Delta w_2 = \xi_2, & \text{in } \Omega_2, \\ \frac{\partial w_1}{\partial \boldsymbol{n}_1} + \epsilon_r\frac{\partial w_2}{\partial \boldsymbol{n}_2} = 0, & \text{on } \Gamma_2, \\ w_1 = w_2, & \text{on } \Gamma_2, \\ \Delta w_1 = 0, & \text{on } \partial\Omega_1, \\ w_1 = 0, & \text{on } \partial\Omega_1 \setminus \Gamma_2, \\ w_2 = 0, & \text{on } \partial\Omega_2 \setminus \Gamma_2, \end{cases} \tag{16}$$

for any $\xi_1 \in L^2(\Omega_1)$, $\xi_2 \in L^2(\Omega_2)$. By means of a similar argument for (7), we know (16) exists a unique solution $w_1 \in H^4(\Omega_1)$ and $w_2 \in H^2(\Omega_2)$ that satisfies the following regularity property:

$$\|w_1\|_{H^4(\Omega_1)} + \|w_2\|_{H^2(\Omega_2)} \le C\left(\|\xi_1\|_{L^2(\Omega_1)} + \|\xi_2\|_{L^2(\Omega_2)}\right). \tag{17}$$

The well-posedness of (16) and the validation of (17) are further discussed in Remark 2.2.

Subtract (11) from (10), yields the following error equations:

$$\left\{\begin{aligned} &(\nabla(\phi_1-\phi_{1,h}),\nabla\tilde{\phi}_1)_{\Omega_1}+\epsilon_r(\nabla(\phi_2-\phi_{2,h}),\nabla\tilde{\phi}_2)_{\Omega_2}=(u-u_h,\tilde{\phi}_1)_{\Omega_1},\\ &\qquad\qquad\qquad\qquad\qquad\qquad\qquad\qquad\forall(\tilde{\phi}_1,\tilde{\phi}_2)\in\boldsymbol{Q_h^0},\\ &\delta_c^2(\nabla(u-u_h),\nabla\tilde{u})_{\Omega_1}+(u-u_h,\tilde{u})_{\Omega_1}=(\rho(\phi_1)-\rho(\phi_{1,h}),\tilde{u})_{\Omega_1},\ \forall\tilde{u}\in W_h^0.\end{aligned}\right.\tag{18}$$

Take $(\xi_1,\xi_2)=(\phi_1-\phi_{1,h},\phi_2-\phi_{2,h})$ in (16), leads to

$$\begin{aligned}||\xi_1||^2_{L^2(\Omega_1)}+||\xi_2||^2_{L^2(\Omega_2)}=&\delta_c^2(\xi_1,\Delta^2w_1)_{\Omega_1}-(\xi_1,\Delta w_1)_{\Omega_1}\\ &-(\xi_1,\rho'(\phi_1)w_1)_{\Omega_1}-\epsilon_r(\xi_2,\Delta w_2)_{\Omega_2}\\ :=&\sum_{i=1}^4 M_i.\end{aligned}\tag{19}$$

Let $(\tilde{\phi}_1,\tilde{\phi}_2)=(\Pi_h\Delta w_1,0)\in\boldsymbol{Q_h^0}$ in $(18)_1$. Then M_1 can be reformulated as

$$\begin{aligned}M_1=&-\delta_c^2(\nabla\xi_1,\nabla(\Delta w_1))_{\Omega_1}\\ =&-\delta_c^2(\nabla\xi_1,\nabla(\Delta w_1-\Pi_h(\Delta w_1)))_{\Omega_1}-\delta_c^2(\nabla\xi_1,\nabla(\Pi_h(\Delta w_1)))_{\Omega_1}\\ \text{by } (18)_1=&-\delta_c^2(\nabla\xi_1,\nabla(\Delta w_1-\Pi_h(\Delta w_1)))_{\Omega_1}-\delta_c^2(u-u_h,\Pi_h(\Delta w_1))_{\Omega_1}\\ =&-\delta_c^2(\nabla\xi_1,\nabla(\Delta w_1-\Pi_h(\Delta w_1)))_{\Omega_1}-\delta_c^2(u-u_h,\Pi_h(\Delta w_1)-\Delta w_1)_{\Omega_1}\\ &+\delta_c^2(\nabla(u-u_h),\nabla w_1)_{\Omega_1}\\ :=&\sum_{j=1}^3 M_{1,j}.\end{aligned}$$

Let $(\tilde{\phi}_1,\tilde{\phi}_2)=(\Pi_h w_1,\Pi_h w_2)\in\boldsymbol{Q_h^0}$ in $(18)_1$, M_2 and M_4 can then be estimated together as follows,

$$\begin{aligned}M_2+M_4=&-(\xi_1,\Delta w_1)_{\Omega_1}-\epsilon_r(\xi_2,\Delta w_2)_{\Omega_2}\\ =&(\nabla\xi_1,\nabla w_1)_{\Omega_1}-<\xi_1,\nabla w_1\cdot n_1>_{\Gamma_2}+\epsilon_r(\nabla\xi_2,\nabla w_2)_{\Omega_2}\\ &-\epsilon_r<\xi_2,\nabla w_2\cdot n_2>_{\Gamma_2}\\ (\text{by } \xi_1|_{\Gamma_2}=\xi_2|_{\Gamma_2}\ \textit{and}\ (16)_3)=&(\nabla\xi_1,\nabla(w_1-\Pi_hw_1))_{\Omega_1}+(\nabla\xi_1,\nabla\Pi_hw_1)_{\Omega_1}\\ &+\epsilon_r(\nabla\xi_2,\nabla(w_2-\Pi_hw_2))_{\Omega_2}+\epsilon_r(\nabla\xi_2,\nabla\Pi_hw_2)_{\Omega_2}\\ (\text{by } (18)_1)=&(\nabla\xi_1,\nabla(w_1-\Pi_hw_1))_{\Omega_1}+\epsilon_r(\nabla\xi_2,\nabla(w_2-\Pi_hw_2))_{\Omega_2}\\ &+(u-u_h,\Pi_hw_1)_{\Omega_1}\\ :=&\sum_{k=1}^3 M_{2,k}.\end{aligned}$$

By Cauchy-Schwartz inequality and regularity property (17), $M_{1,j}$ $(j = 1, 2, 3)$ can be estimated as follows,

$$\begin{aligned}
M_{1,1} \leq & Ch\|\nabla\xi_1\|_{L^2(\Omega_1)}\|w_1\|_{H^4(\Omega_1)} \\
\leq & Ch\|\nabla\xi_1\|_{L^2(\Omega_1)}\left(\|\xi_1\|_{L^2(\Omega_1)} + \|\xi_2\|_{L^2(\Omega_2)}\right), \\
M_{1,2} \leq & Ch^2\|u - u_h\|_{L^2(\Omega_1)}\|w_1\|_{H^4(\Omega_1)} \\
\leq & Ch^2\|u - u_h\|_{L^2(\Omega_1)}\left(\|\xi_1\|_{L^2(\Omega_1)} + \|\xi_2\|_{L^2(\Omega_2)}\right), \\
M_{1,3} = & \delta_c^2(\nabla(u - u_h), \nabla(w_1 - \Pi_h w_1))_{\Omega_1} + \delta_c^2(\nabla(u - u_h), \nabla\Pi_h w_1)_{\Omega_1} \\
(\text{by}(18)_2) \quad = & \delta_c^2(\nabla(u - u_h), \nabla(w_1 - \Pi_h w_1))_{\Omega_1} \\
& - (u - u_h, \Pi_h w_1)_{\Omega_1} + (\rho(\phi_1) - \rho(\phi_{1,h}), \Pi_h w_1)_{\Omega_1} \\
= & \delta_c^2(\nabla(u - u_h), \nabla(w_1 - \Pi_h w_1))_{\Omega_1} - (u - u_h, \Pi_h w_1)_{\Omega_1} \\
& + (\rho(\phi_1) - \rho(\phi_{1,h}), \Pi_h w_1 - w_1)_{\Omega_1} + (\rho(\phi_1) - \rho(\phi_{1,h}), w_1)_{\Omega_1} \\
:= & \sum_{l=1}^{4} M_{1,3,l}.
\end{aligned}$$

Then by the Mean Value Theorem and Lipschitz continuities of $\rho(\cdot)$ and its derivatives, we can obtain

$$\begin{aligned}
M_{1,3,3} = & (\rho'(\eta_1)(\phi_1 - \phi_{1,h}), \Pi_h w_1 - w_1)_{\Omega_1} \\
\leq & C\|\xi_1\|_{L^2(\Omega_1)}\|\Pi_h w_1 - w_1\|_{L^2(\Omega_1)} \\
\leq & Ch^4\|\xi_1\|_{L^2(\Omega_1)}\left(\|\xi_1\|_{L^2(\Omega_1)} + \|\xi_2\|_{L^2(\Omega_2)}\right),
\end{aligned} \tag{20}$$

and

$$\begin{aligned}
M_{1,3,4} + M_3 = & (\rho'(\eta_1)\xi_1, w_1)_{\Omega_1} - (\xi_1, \rho'(\phi_1)w_1)_{\Omega_1} \\
\leq & |(\rho''(\eta_2)(\eta_1 - \phi_1)\xi_1, w_1)_{\Omega_1}| \\
\leq & C\|\xi_1\|^2_{L^2(\Omega_1)}\|w_1\|_{L^\infty(\Omega_1)} \\
\leq & C\|\xi_1\|^2_{L^2(\Omega_1)}\|w_1\|_{H^4(\Omega_1)},
\end{aligned} \tag{21}$$

where η_1, η_2 fall in between ϕ_1 and $\phi_{1,h}$, and $||w_1||_{L^\infty(\Omega_1)} \leq C||w_1||_{H^4(\Omega_1)}$ is applied.

By Cauchy-Schwartz inequality, $M_{2,k}$ $(k = 1, 2)$ and $M_{1,3,1}$ can be obtained as follows,

$$\begin{aligned}
M_{2,1} \leq & Ch^3\|\nabla\xi_1\|_{L^2(\Omega_1)}\left(\|\xi_1\|_{L^2(\Omega_1)} + \|\xi_2\|_{L^2(\Omega_2)}\right), \\
M_{2,2} \leq & Ch\|\nabla\xi_2\|_{L^2(\Omega_2)}\left(\|\xi_1\|_{L^2(\Omega_1)} + \|\xi_2\|_{L^2(\Omega_2)}\right), \\
M_{1,3,1} \leq & Ch^3\|\nabla(u - u_h)\|_{L^2(\Omega_1)}\left(\|\xi_1\|_{L^2(\Omega_1)} + \|\xi_2\|_{L^2(\Omega_2)}\right).
\end{aligned}$$

Finally, $M_{1,3,2}$ cancels $M_{2,3}$, then combine the above estimates, apply the regularity property (17) and ε-Young's inequality, (19) can be estimated as

$$\begin{aligned}
& \|\xi_1\|_{L^2(\Omega_1)} + \|\xi_2\|_{L^2(\Omega_2)} \\
\leq & C\Big(h^2\|u - u_h\|_{L^2(\Omega_1)} + h^3\|\nabla(u - u_h)\|_{L^2(\Omega_1)} + h^4\|\xi_1\|_{L^2(\Omega_1)} \\
& + (h^3 + h)\|\nabla\xi_1\|_{L^2(\Omega_1)} + h\|\nabla\xi_2\|_{L^2(\Omega_2)} + \|\xi_1\|^2_{L^2(\Omega_1)}\Big),
\end{aligned}$$

which directly leads to the desired (15). □

Remark 2.2. *We further demonstrate the well-posedness of (16) and its regularity property (17) below. First, we equivalently reformulate (16) to the following two subproblems:*

$$
\text{(I)} \begin{cases} -\Delta w_1 = v, & \text{in } \Omega_1, \\ -\epsilon_r \Delta w_2 = \xi_2, & \text{in } \Omega_2, \\ \frac{\partial w_1}{\partial \boldsymbol{n}_1} + \epsilon_r \frac{\partial w_2}{\partial \boldsymbol{n}_2} = 0, & \text{on } \Gamma_2, \\ w_1 = w_2, & \text{on } \Gamma_2, \\ w_1 = 0, & \text{on } \partial\Omega_1 \setminus \Gamma_2, \\ w_2 = 0, & \text{on } \partial\Omega_2 \setminus \Gamma_2, \end{cases}
$$

$$
\text{(II)} \begin{cases} -\delta_c^2 \Delta v + v = \rho'(\phi_1) w_1 + \xi_1, & \text{in } \Omega_1, \\ v = 0, & \text{on } \partial\Omega_1. \end{cases}
$$

Clearly, the subproblem (I) is an elliptic interface equation whose well-posedness has been studied in [24] when the interface Γ_2 is C^2-smooth, so we assume the following regularity inequality holds [24]:

$$
\|w_1\|_{H^2(\Omega_1)} + \|w_2\|_{H^2(\Omega_2)} \le C \left(\|v\|_{L^2(\Omega_1)} + \|\xi_2\|_{L^2(\Omega_2)} \right). \tag{22}
$$

On the other hand, the subproblem (II) is a nonlinear elliptic equation defined in a single domain Ω_1 with a homogeneous Dirichlet boundary condition, due to the nonlinear term $\rho'(\phi_1)w_1$ on the right hand side that essentially depends on v from the first equation of subproblem (I). Considering that the regularity theory of nonlinear elliptic equation has been long studied for many cases (e.g., see [42, 43, 44, 45]), we may safely assume the following regularity inequality for the subproblem (II):

$$
\|v\|_{H^2(\Omega_1)} \le C \|\xi_1\|_{L^2(\Omega_1)}. \tag{23}
$$

Combine (22) and (23), apply $\|v\|_{L^2(\Omega_1)} \le C\|v\|_{H^2(\Omega_1)}$ and $\|w_1\|_{H^4(\Omega_1)} \cong \|v\|_{H^2(\Omega_1)}$, the regularity inequality (17) can thus be attained.

Next, we derive the main result of this paper: the optimal error convergence of the developed FEM in both H^1 and L^2 norms for the presented fourth-order/second-order Poisson-Fermi interface problem.

Theorem 2.1. *Let (ϕ_1, ϕ_2, u) be the solution of (10) and $(\phi_{1,h}, \phi_{2,h}, u_h)$ be the solution of (11). Assume regularity properties $\phi_1 \in H^{k+3}(\Omega_1)$ and $\phi_2 \in H^{k+1}(\Omega_2)$ are held. Then the following optimal error estimates hold*

$$
\begin{aligned}
&\|\phi_1 - \phi_{1,h}\|_{L^2(\Omega_1)} + h\|\phi_1 - \phi_{1,h}\|_{H^1(\Omega_1)} + \|\phi_2 - \phi_{2,h}\|_{L^2(\Omega_2)} \\
&+ h\|\phi_2 - \phi_{2,h}\|_{H^1(\Omega_2)} + \|u - u_h\|_{L^2(\Omega_1)} + h\|u - u_h\|_{H^1(\Omega_1)} \le Ch^{k+1}.
\end{aligned} \tag{24}
$$

Proof. Firstly, we need to define the H^1-projection of $u \in W$, $P_h u \in W_h$ such that

$$
\delta_c^2 (\nabla(u - P_h u), \nabla \tilde{u})_{\Omega_1} + (u - P_h u, \tilde{u})_{\Omega_1} = 0, \ \forall \tilde{u} \in W_h^0. \tag{25}
$$

It is well known that the following error estimates hold [41]

$$
\|u - P_h u\|_{L^2(\Omega_1)} + h\|u - P_h u\|_{H^1(\Omega_1)} \le Ch^{k+1} \|u\|_{H^{k+1}(\Omega_1)}. \tag{26}
$$

Then, subtract $(11)_2$ from $(10)_2$ and apply (25), yield

$$
\delta_c^2 (\nabla(P_h u - u_h), \nabla \tilde{u})_{\Omega_1} + (P_h u - u_h, \tilde{u})_{\Omega_1} = (\rho(\phi_1) - \rho(\phi_{1,h}), \tilde{u}), \ \forall \tilde{u} \in W_h^0. \tag{27}
$$

Let $\tilde{u} = P_h u - u_h$ in (27), apply ε-Young's inequality with an appropriately small $\varepsilon > 0$, yield

$$\begin{aligned}
&\delta_c^2 \|\nabla(P_h u - u_h)\|^2_{L^2(\Omega_1)} + \|P_h u - u_h\|^2_{L^2(\Omega_1)} \\
=&(\rho(\phi_1) - \rho(\phi_{1,h}), P_h u - u_h) \\
=&(\rho'(\eta)(\phi_1 - \phi_{1,h}), P_h u - u_h) \\
\leq& C\|\phi_1 - \phi_{1,h}\|^2_{L^2(\Omega_1)} + \varepsilon \|P_h u - u_h\|^2_{L^2(\Omega_1)}.
\end{aligned}$$

Then by (26), we obtain

$$\|u - u_h\|_{L^2(\Omega_1)} + h\|\nabla(u - u_h)\|_{L^2(\Omega_1)} \leq C\left(h^{k+1} + \|\phi_1 - \phi_{1,h}\|_{L^2(\Omega_1)}\right). \tag{28}$$

Let $(\tilde{\phi}_1, \tilde{\phi}_2) = (\Pi_h\phi_1 - \phi_{1,h}, \Pi_h\phi_2 - \phi_{2,h}) \in \boldsymbol{Q_h^0}$ in $(18)_1$, we have

$$\begin{aligned}
&\|\nabla(\Pi_h\phi_1 - \phi_{1,h})\|^2_{L^2(\Omega_1)} + \epsilon_r\|\nabla(\Pi_h\phi_2 - \phi_{2,h})\|^2_{L^2(\Omega_2)} \\
=&(u - u_h, \Pi_h\phi_1 - \phi_{1,h})_{\Omega_1} - (\nabla(\phi_1 - \Pi_h\phi_1), \nabla(\Pi_h\phi_1 - \phi_{1,h})) \\
&- \epsilon_r(\nabla(\phi_2 - \Pi_h\phi_2), \nabla(\Pi_h\phi_2 - \phi_{2,h})) \\
\leq& C\left(\|u - u_h\|^2_{L^2(\Omega_1)} + \|\Pi_h\phi_1 - \phi_{1,h}\|^2_{L^2(\Omega_1)}\right) \\
&+ C\left(\|\nabla(\phi_1 - \Pi_h\phi_1)\|^2_{L^2(\Omega_1)} + \|\nabla(\phi_2 - \Pi_h\phi_2)\|^2_{L^2(\Omega_2)}\right) \\
&+ \epsilon\left(\|\nabla(\Pi_h\phi_1 - \phi_{1,h})\|^2_{L^2(\Omega_1)} + \|\nabla(\Pi_h\phi_2 - \phi_{2,h})\|^2_{L^2(\Omega_2)}\right).
\end{aligned}$$

Thus, choosing an appropriately small ε, we have

$$\begin{aligned}
&\|\nabla(\Pi_h\phi_1 - \phi_{1,h})\|_{L^2(\Omega_1)} + \epsilon_r\|\nabla(\Pi_h\phi_2 - \phi_{2,h})\|_{L^2(\Omega_2)} \\
\leq& C\left(\|u - u_h\|_{L^2(\Omega_1)} + \|\Pi_h\phi_1 - \phi_{1,h}\|_{L^2(\Omega_1)} + h^k\right).
\end{aligned} \tag{29}$$

Substitute (28) and (29) into (15), yields

$$\begin{aligned}
\|\phi_1 - \phi_{1,h}\|_{L^2(\Omega_1)} + \|\phi_2 - \phi_{2,h}\|_{L^2(\Omega_2)} \leq& C\left(h^{k+3} + (h^2 + h)\|\phi_1 - \phi_{1,h}\|_{L^2(\Omega_1)}\right. \\
&\left.+ h^{k+2} + h^{k+1} + \|\phi_1 - \phi_{1,h}\|^2_{L^2(\Omega_1)}\right).
\end{aligned}$$

Via a similar compactness argument [46], we have $\phi_{1,h} \to \phi_1$ in $L^2(\Omega_1)$ as $h \to 0$ (see the proof in Remark 2.3). Hence $\|\phi_1 - \phi_{1,h}\|_{L^2(\Omega_1)} \to 0$ as $h \to 0$, leading to

$$\|\phi_1 - \phi_{1,h}\|_{L^2(\Omega_1)} + \|\phi_2 - \phi_{2,h}\|_{L^2(\Omega_2)} \leq Ch^{k+1}. \tag{30}$$

By (28) and (30), we have

$$\|u - u_h\|_{L^2(\Omega_1)} + h\|\nabla(u - u_h)\|_{L^2(\Omega_1)} \leq Ch^{k+1}. \tag{31}$$

Then by (29), we can get

$$\|\nabla(\phi_1 - \phi_{1,h})\|_{L^2(\Omega_1)} + \|\nabla(\phi_2 - \phi_{2,h})\|_{L^2(\Omega_2)} \leq Ch^k. \tag{32}$$

Combining (30), (31) and (32), we then obtain the desired result. □

Remark 2.3. *By an analogous compactness argument [46], we can prove $\phi_{1,h} \to \phi_1$ in $L^2(\Omega_1)$ as $h \to 0$, as shown below. We first prove the boundedness of $\phi_{1,h}$ and u_h in $H^1(\Omega_1)$, and of $\phi_{2,h}$ in $H^1(\Omega_2)$. Let $\tilde{\phi}_1 = \phi_{1,h}, \tilde{\phi}_2 = \phi_{2,h}$ and $\tilde{u} = u_h$ in (11). By Cauchy-Schwartz inequality, Poincáre inequality, and the boundedness of $\rho(\cdot)$, we can easily obtain*

$$\|\phi_{1,h}\|_{H^1(\Omega_1)} + \|\phi_{2,h}\|_{H^1(\Omega_2)} + \|u_h\|_{H^1(\Omega_1)} \leq C, \tag{33}$$

where C is independent of h but is dependent of the boundedness of known functions f_1, f_2, g, g_1, g_2, g_3, g_4 and ρ in their respective norms, appropriately. As a consequence of Eberlein-Schmulyan theorem, (33) induces that we can choose a subsequence $\{h_k\}_{k=0}^{\infty}$ from any sequence of h's tending to zero such that for some $\omega_1 \in H^1(\Omega_1)$, $\omega_2 \in H^1(\Omega_2)$ and $\omega \in H^1(\Omega_1)$, $\phi_{1,h_k} \to \omega_1$, $u_{h_k} \to \omega$ in $L^2(\Omega_1)$ and weakly in $H^1(\Omega_1)$, $\phi_{2,h_k} \to \omega_2$ in $L^2(\Omega_2)$ and weakly in $H^1(\Omega_2)$. We wish to demonstrate that $\omega_1 \equiv \phi_1$, $\omega_2 \equiv \phi_2$ and $\omega \equiv u$, which is the solution of (10). To the end, we let $\tilde{\phi}_1 \in C_0^\infty(\Omega_1)$, $\tilde{\phi}_2 \in C_0^\infty(\Omega_2)$ and $\tilde{u} \in C_0^\infty(\Omega_1)$. Then $(\Pi_h\tilde{\phi}_1, \Pi_h\tilde{\phi}_2) \in \boldsymbol{Q_h^0}$ and $\Pi_h\tilde{u} \in W_h^0$, leading to: $\|\tilde{\phi}_1 - \Pi_h\tilde{\phi}_1\|_{H^1(\Omega_1)} \to 0$, $\|\tilde{\phi}_2 - \Pi_h\tilde{\phi}_2\|_{H^1(\Omega_2)} \to 0$ and $\|\tilde{u} - \Pi_h\tilde{u}\|_{H^1(\Omega_1)} \to 0$ as $h \to 0$. Therefore, by (10) we have

$$
\begin{aligned}
&\Big|(\nabla\omega_1, \nabla\tilde{\phi}_1)_{\Omega_1} + \epsilon_r(\nabla\omega_2, \nabla\tilde{\phi}_2)_{\Omega_2} + \delta_c^2(\nabla\omega, \nabla\tilde{u})_{\Omega_1} + (\omega, \tilde{u})_{\Omega_1} - (\omega, \tilde{\phi}_1)_{\Omega_1} \\
&\quad -(\rho(\omega_1), \tilde{u})_{\Omega_1} - < g_2, \tilde{\phi}_1 >_{\Gamma_2} - < g_3, \tilde{\phi}_1 >_{\Gamma} -(f_2, \tilde{\phi}_2)_{\Omega_2} - (f_1, \tilde{u})_{\Omega_1}\Big| \\
\le&|(\nabla(\omega_1 - \phi_{1,h_k}), \nabla\tilde{\phi}_1)_{\Omega_1}| + |(\nabla\phi_{1,h_k}, \nabla(\tilde{\phi}_1 - \Pi_h\tilde{\phi}_1))_{\Omega_1}| \\
&+ \epsilon_2|(\nabla(\omega_2 - \phi_{2,h_k}), \nabla\tilde{\phi}_2)_{\Omega_2}| + \epsilon_2|(\nabla\phi_{2,h_k}, \nabla(\tilde{\phi}_2 - \Pi_h\tilde{\phi}_2))_{\Omega_2}| \\
&+ \delta_c^2|(\nabla(\omega - u_{h_k}), \nabla\tilde{u})_{\Omega_1}| + \delta_c^2|(\nabla u_{h_k}, \nabla(\tilde{u} - \Pi_h\tilde{u}))_{\Omega_1}| \\
&+ |(\omega - u_{h_k}, \tilde{u})_{\Omega_1}| + |(u_{h_k}, \tilde{u} - \Pi_h\tilde{u})_{\Omega_1}| + |(\omega - u_{h_k}, \tilde{\phi}_1)_{\Omega_1}| \\
&+ |(u_{h_k}, \Pi_h\tilde{\phi}_1 - \tilde{\phi}_1)_{\Omega_1}| + | < g_2, \Pi_h\tilde{\phi}_1 - \tilde{\phi}_1 >_{\Gamma_2} | \\
&+ | < g_3, \Pi_h\tilde{\phi}_1 - \tilde{\phi}_1 >_{\Gamma} | + |(f_2, \Pi_h\tilde{\phi}_2 - \tilde{\phi}_2)_{\Omega_2}| \\
&+ |(f_1, \Pi_h\tilde{u} - \tilde{u})_{\Omega_1}| + |(\rho(\omega_1), \Pi_h\tilde{u} - \tilde{u})_{\Omega_1}| + |(\rho(\phi_{1,h_k}) - \rho(\omega_1)), \Pi_h\tilde{u})_{\Omega_1}| \\
\le& C\big(\|\omega_1 - \phi_{1,h_k}\|_{H^1(\Omega_1)}\|\tilde{\phi}_1\|_{H^1(\Omega_1)} + \|\phi_{1,h_k}\|_{H^1(\Omega_1)}\|\tilde{\phi}_1 - \Pi_h\tilde{\phi}_1\|_{H^1(\Omega_1)} \\
&+ \|\omega_2 - \phi_{2,h_k}\|_{H^1(\Omega_2)}\|\tilde{\phi}_2\|_{H^1(\Omega_2)} + \|\phi_{2,h_k}\|_{H^1(\Omega_2)}\|\tilde{\phi}_2 - \Pi_h\tilde{\phi}_2\|_{H^1(\Omega_2)} \\
&+ \|\omega - u_{h_k}\|_{H^1(\Omega_1)}\|\tilde{u}\|_{H^1(\Omega_1)} + \|u_{h_k}\|_{H^1(\Omega_1)}\|\tilde{u} - \Pi_h\tilde{u}\|_{H^1(\Omega_1)} \\
&+ \|\omega - u_{h_k}\|_{L^2(\Omega_1)}\|\tilde{\phi}_1\|_{L^2(\Omega_1)} + \|u_{h_k}\|_{L^2(\Omega_1)}\|\Pi_h\tilde{\phi}_1 - \tilde{\phi}_1\|_{L^2(\Omega_1)} \\
&+ \|\Pi_h\tilde{\phi}_1 - \tilde{\phi}_1\|_{H^1(\Omega_1)} + \|\Pi_h\tilde{\phi}_2 - \tilde{\phi}_2\|_{L^2(\Omega_2)} + \|\Pi_h\tilde{u} - \tilde{u}\|_{L^2(\Omega_1)} \\
&+ \|\phi_{1,h_k} - \omega_1\|_{L^2(\Omega_1)}\|\Pi_h\tilde{u}\|_{L^2(\Omega_1)}\big) \\
&\qquad \to 0, \quad \text{as } h \to 0,
\end{aligned}
$$

where the trace inequality is applied to $\|\Pi_h\tilde{\phi}_1 - \tilde{\phi}_1\|_{L^2(\partial\Omega_1)}$. Thus, by $\overline{C_0^\infty(\Omega_i)} = H_0^1(\Omega_i)$ for $i = 1, 2$, we know ω_1, ω_2 and ω is the solution of (10). From the uniqueness of solution of (10) it follows that $\omega_1 \equiv \phi_1$, $\omega_2 \equiv \phi_2$ and $\omega \equiv u$. Hence, $\|\phi_1 - \phi_{1,h}\|_{L^2(\Omega_1)} \to 0$ as $h \to 0$.

Remark 2.4. *For simplicity, in this paper we assume that both Ω_1 and Ω_2 are polygonal or polyhedral convex domain in $\mathbb{R}^d$ $(d = 2, 3)$, which means the interface Γ_2 is formed by polyline or polygon, accordingly. Thus, the triangulation $\mathcal{T}_h$ exactly fills up the entire domain Ω while fitting the interface Γ_2, exactly. We refer to* [24] *where a more general case was considered, i.e., the interface Γ_2 holds the regularity of C^2. In this general case, we need to consider a geometric approximation to the smooth interface Γ_2, which can be estimated through an analogous analysis process as done in* [24]. *We avoid those geometry-related approximation errors for the general case by focusing our efforts on the more important point in this paper: numerical treatment and theoretical analysis via interface conditions of the* *fourth-/second-order Poisson-Fermi interface problem in the frame of finite element approximation.*

2.3.1. The Maxwell tensor. The Maxwell's stress tensor in the non-local electrolyte (the solvent subdomain) can be expressed as follows [47]:

$$\begin{aligned}\boldsymbol{\tau} =& \epsilon \boldsymbol{q}\boldsymbol{q}^T - \frac{1}{2}\epsilon \boldsymbol{q}^T\boldsymbol{q}\boldsymbol{I} \\ &+ \epsilon l_c^2\left[(\nabla(\nabla\cdot\boldsymbol{q}))^T\boldsymbol{q}\boldsymbol{I} - \boldsymbol{q}(\nabla(\nabla\cdot\boldsymbol{q}))^T - (\nabla(\nabla\cdot\boldsymbol{q}))\boldsymbol{q}^T + \frac{1}{2}(\nabla\cdot\boldsymbol{q})^2\boldsymbol{I}\right],\end{aligned} \tag{34}$$

where $\boldsymbol{q} = -\nabla\phi_1$ denotes the electric field in the solvent subdomain Ω_1, and $\boldsymbol{I}$ is the identity martix. Thus by $(8)_1$, we know $\nabla\cdot\boldsymbol{q} = -u$ in Ω_1.

The following corollary defines a finite element approximation to Maxwell's stress tensor defined in (34), and demonstrates a corresponding error estimation that can be similarly proved as done in [35] and is thus omitted here.

Corollary 2.1. *Let $(\phi_{1,h}, u_h)$ be the solution to (11). Then the Maxwell's stress tensor $\boldsymbol{\tau} \in [\boldsymbol{H(div;\Omega_1)}]^d := \{\boldsymbol{v} \in [L^2(\Omega_1)]^{d\times d} : \nabla\cdot\boldsymbol{v} \in [L^2(\Omega_1)]^d\}$ in (34) can be piecewisely approximated by the following discrete stress tensor, $\boldsymbol{\tau_h} \in \boldsymbol{\Theta(\Omega_1)} := \{\boldsymbol{v} \in [L^2(\Omega_1)]^{d\times d} : \boldsymbol{v}|_K \in [\boldsymbol{H(div;\Omega_1)}]^d, \forall K \in \mathcal{T}_h\}$*

(35)

$$\begin{aligned}\boldsymbol{\tau}_h =& \epsilon(\nabla\phi_{1,h})(\nabla\phi_{1,h})^T - \frac{1}{2}\epsilon(\nabla\phi_{1,h})^T(\nabla\phi_{1,h})\boldsymbol{I} \\ &+ \epsilon l_c^2\left[-(\nabla u_h)^T(\nabla\phi_{1,h})\boldsymbol{I} + (\nabla\phi_{1,h})(\nabla u_h)^T + (\nabla u_h)(\nabla\phi_{1,h})^T + \frac{1}{2}u_h^2\boldsymbol{I}\right],\end{aligned}$$

and the follwing error estimate holds

$$\|\boldsymbol{\tau} - \boldsymbol{\tau}_h\|_{L^2(\Omega_1)} \le Ch^k, \tag{36}$$

under an additional regularity assumption: $\phi_1 \in H^{k+3}(\Omega_1) \cap W^{1,\infty}(\Omega_1)$.

3. Numerical experiments

3.1. Example 1: Convergence test for the back to back case. We take the following function as the exact solution of (7) by appropriately defining f_1, f_2, g_1, g_2, g_3, g_4 and g,

$$\begin{cases} \phi_1 = x^2(y^2-1)e^{(x+y)}, \\ \phi_2 = x^2(y^2+1)e^{(x+y)}, \end{cases} \tag{37}$$

where we choose $\Omega := [-1,1]\times[-1,1], \Omega_1 := [-1,0]\times[-1,1]$, $\Omega_2 = \Omega\backslash\Omega_1$ (see Fig. 3), and $\varepsilon_r = 2$, $\delta_c = 1$, $\rho(\phi_1) = \frac{e^{-z_1\phi_1} - e^{-z_2\phi_1}}{z_1 - z_2}$ with $z_1 = 1, z_2 = -1$. Finite element spaces $\boldsymbol{Q_h}$ and W_h are defined by taking $k = 1$. Then based upon a grid doubling strategy in which the mesh sizes $h = h_1 = h_2 = 1/16, 1/32, 1/64$ and $1/128$ are taken in turns, we implement Algorithm 1 while letting the tolerance $\varsigma = 10^{-12}$ in (14). Numerical results of the finite element approximation to (ϕ_1, ϕ_2, u) are reported in Table 1 and Fig. 4, showing that all numerical convergence rates are optimal, which are in accordance with theoretical results shown in Theorem 2.1.

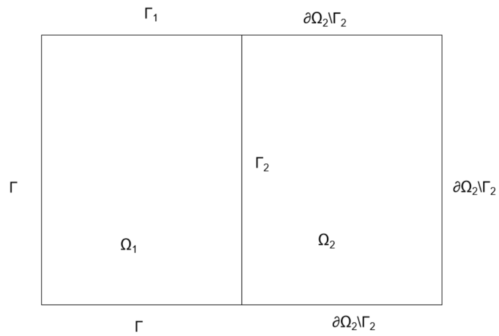

FIGURE 3. Schematic domain of the back to back case.

TABLE 1. Convergence results of Example 1.

h	1/16	1/32	1/64	1/128
$\|\phi_1 - \phi_{1,h}\|_{L^2(\Omega_1)}$	4.614E-03	1.280E-03	3.267E-04	8.136E-05
Order		1.85	1.97	2.01
$\|\phi_1 - \phi_{1,h}\|_{H^1(\Omega_1)}$	5.858E-02	2.942E-02	1.468E-02	7.329E-03
Order		0.99	1.00	1.00
$\|\phi_2 - \phi_{2,h}\|_{L^2(\Omega_2)}$	2.870E-02	7.353E-03	2.035E-03	4.989E-04
Order		1.96	1.85	2.03
$\|\phi_2 - \phi_{2,h}\|_{H^1(\Omega_2)}$	1.286	6.551E-01	3.298E-01	1.643E-01
Order		0.97	0.99	1.00
$\|u - u_h\|_{L^2(\Omega_1)}$	1.092E-02	2.826E-03	7.320E-04	1.835E-04
Order		1.95	1.95	2.00
$\|u - u_h\|_{H^1(\Omega_1)}$	5.076E-01	2.561E-01	1.263E-01	6.330E-02
Order		0.99	1.02	1.00

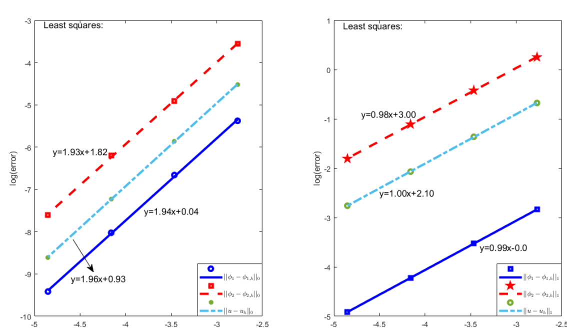

FIGURE 4. Linear least squares fitting of convergence trends of Example 1.

TABLE 2. Convergence results of Example 2.

h	1/16	1/32	1/64	1/128
$\Vert\phi-\phi_h\Vert_{L^2(\Omega)}$	2.374E-01	6.079E-02	1.615E-02	4.131E-03
Order		1.97	1.91	1.97
$\Vert\phi-\phi_h\Vert_{H^1(\Omega)}$	6.763E-01	3.375E-01	1.741E-01	8.755E-02
Order		1.00	0.96	0.99
$\Vert u-u_h\Vert_{L^2(\Omega_1)}$	3.459E-01	8.297E-02	2.194E-02	5.590E-03
Order		2.06	1.92	1.97
$\Vert u-u_h\Vert_{H^1(\Omega_1)}$	1.269	6.496E-01	3.370E-01	1.701E-01
Order		0.97	0.95	0.99

Furthermore, we illustrate the convergence performance of Algorithm 1, numerically, in Fig. 5, showing that the Picard's iteration converges within only nine iteration steps, with the stop criterion (14) and the tolerance $\varsigma = 10^{-12}$.

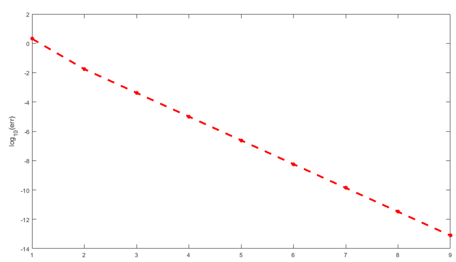

FIGURE 5. Convergence history of Picard's iteration for Example 1: iterative errors versus iteration steps n.

3.2. Example 2: Convergence test for the immersed case. We take the following function as the exact solution of (7) by appropriately defining the right hand side function of each equation in (7),

$$\phi_1 = \phi_2 = \sin(x)\sin(y),$$

where we choose $\Omega := \{(x,y)|x^2+y^2 < R_1^2, y \geq 0\}$, $\Omega_2 := \{(x,y)|x^2+(y-dL-R_2)^2 < R_2^2\}$ with $R_1 = 3.0$, $R_2 = 1.0$, $dL = 0.5$, $\Omega_1 = \Omega\backslash\Omega_2$ (see Fig. 1), and the same parameters and $\rho(\phi_1)$ as chosen in Example 1. We employ the same finite element spaces and the same mesh size sequences as used for Example 1 to investigate finite element convergence rates by implementing Algorithm 1 through the grid doubling process. Numerical results of the finite element approximation to (ϕ_1, ϕ_2, u) are reported in Table 2 and Fig. 6, where errors of $(\phi_1 - \phi_{1,h})$ and of $(\phi_2 - \phi_{2,h})$ are combined together and represented as the error of $(\phi - \phi_h)$ in either L^2 or H^1 norm, showing that all numerical convergence rates are optimal that agree with Theorem 2.1. Moreover, we test the convergence result of the Maxwell's stress tensor $\boldsymbol{\tau}$ that occurs in Ω_1 only by using (35) to compute the discrete stress tensor $\boldsymbol{\tau}_h$. As shown in Table 3 and Fig. 7, we can see that the convergence rate of $\Vert\boldsymbol{\tau}-\boldsymbol{\tau}_h\Vert_{L^2(\Omega_1)}$ is the first order, which is consistent with Corollary 2.1.

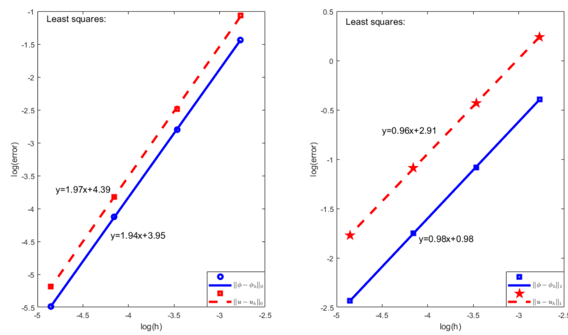

FIGURE 6. Linear least squares fitting of convergence trends of Example 2.

TABLE 3. Convergence results of Maxwell's stress tensor in Example 2.

h	1/16	1/32	1/64	1/128
$\|\boldsymbol{\tau} - \boldsymbol{\tau}_h\|_{L^2(\Omega_1)}$	1.989	1.082	5.761E-01	2.978E-01
Order		0.88	0.91	0.95

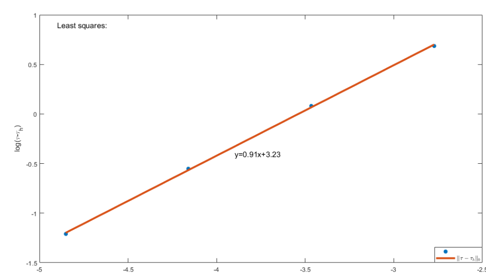

FIGURE 7. Linear least squares fitting of convergence trends of Maxwell's stress tensor in Example 2.

3.3. Example 3: The interactional forces of charged particles immersed in an electrolyte. According to the Coulomb's law, the electrostatic force of interaction among them is counter-proportional to the distance between them. In addition, oppositely charged objects attract each other and vice versa due to the classical theory of electromagnetism. However, in the presence of polyvalent ions, counter-intuitive phenomena occur, such as the mutual attraction of molecules with the same charge, or oppositely charged objects repel each other. Similarly, the electrophoretic mobility of charged colloids is reversed in the presence of multivalent ions. This phenomenon is known as charge reversal or overcharging [48].

Charge reversal occurs when the concentration of the polyvalent ions in the bulk solution increases to some extent. Here, we integrate the total electrostatic force on the surface of the charged particle, Γ_2, that interacts with the charged boundary

Γ_3 by computing the normal Maxwell stress tensor $\boldsymbol{\tau}$ over Γ_2, i.e., $\boldsymbol{F} = \int_{\Gamma_2} \boldsymbol{\tau n} ds$. Due to the symmetry setting, the combination of all horizontal components of the total electrostatic force $\boldsymbol{F}$ equals zero. So we only need to investigate the vertical component of the total electrostatic force. All required physical parameters used in the example are explained and labeled in Table 4.

We carry out Algorithm 1 to solve this physical problem modeled by the presented fourth-order/second-order Poisson-Fermi interface problem. The vertical interactional force in the unit of Nanonewton (nN), $\boldsymbol{F}$, acts on the surface of the particle with respect to the distance from the charged boundary Γ_3, dL, and to the far field concentration of ions in electrolyte, c_0, which equals $\frac{C_\infty^+}{N_A}$ in the unit of mM (i.e., mol/m^3). Numerical results are illustrated in Table 5 and Fig. 8, where we can see that for two oppositely charged objects, the interactional force between them gradually reverses from the mutually attractive (downward) direction to the repulsive (upward) direction, which is in agreement with the change mode of experimental results shown in [48, 49]. In addition, Fig. 8 also shows that as the distance between two charged objects increases, the vertical force between them decreases, which illustrates that the classical Coulomb's law is still held while the charge reversal phenomenon occurs.

TABLE 4. Notation and physical constants in Example 3.

$Notation$	Phisical definition	Value	Unit
R_1	Spherical radius of the electrolyte field	6	nm
R_2	Spherical radius of charge particles	0.09	nm
e	Unit electron charge	1.6×10^{-19}	C
K_BT	Boltzmann energy	4.14×10^{-21}	J (or N m)
ϵ_0	Permittivity of vacuum	8.85×10^{-12}	$\mathrm{C}^2/(\mathrm{N\ m}^2)$
ϵ_s	Electrolyte's dielectric constant	80	
ϵ_m	Particle's dielectric constant	2	
z_1	Valency of cation	3	
z_2	Valency of anion	-1	
l_c	Electrostatic correlation length	1	nm
σ	Surface charge	50	$\mathrm{mV/m}^2$
N_A	Avogadro constant	6.02×10^{23}	mol^{-1}

TABLE 5. Vertical force (nN) acting on the particle in Example 3.

dL(nm)	c_0=15.85 mM	c_0=63.4 mM	c_0=1585.0 mM
2.1	-4.52E-06	-1.19E-06	8.19E-07
2.8	-2.74E-06	-2.20E-07	1.76E-08
3.5	-1.47E-06	-2.19E-07	4.40E-08

4. Conclusion and future work

In this paper, we develop and analyze a type of interface-fitted finite element approximation to the fourth-order/second-order Poisson-Fermi interface problem arising from the BSK theory that is considered as a significant extension of the

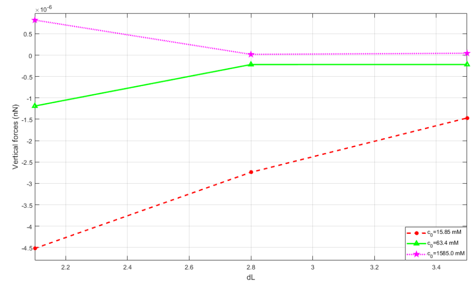

FIGURE 8. Vertical forces (nN) acting on the particle versus ionic concentrations and distances in Example 3.

classical Poisson-Boltzmann theory. Optimal error estimates are obtained for all finite element solutions in their respective subdomains in both H^1 and L^2 norms, where nonhomogeneous interface conditions across the interface of solvent and solute play a key role in the derivation of optimal convergence results. In addition, we also numerically compute the total interactional electrostatic force via its finite element approximation to investigate the charge reversal phenomenon governed by the BSK theory, which is illustrated by numerical experiments that, as the concentration in the electrolyte increases, two oppositely charged particles that attract each other in the first place become mutually exclusive, while the total electrostatic force between two particles is inversely proportional to the distance between them. The developed interface-fitted finite element method can be extended to the case of moving interface problem involving fourth- and/or second-order Poisson-Fermi equations with jump coefficients, where the arbitrary Lagrangian-Eulerian (ALE) method will be employed to generate a connectivity-preserving moving mesh that fits the interface all the time. Then, on the time-dependent moving mesh we will further study the interface-fitted finite element method developed in this paper within the ALE frame, which will be carried out in our next paper.

Acknowledgments

M. He was partially supported by Natural Science Foundation of China (No. 12171366). P. Sun was partially supported by a grant from the Simons Foundation (MPS-706640, PS).

References

[1] W.C.K. Poon and D. Andelman. Soft Condensed Matter Physics in Molecular and Cell Biology. Taylor and Francis, CRC Press, 2006.

[2] C.F. Wong and J.A. McCammon. Protein flexibility and computer-aided drug design. Annual Review of Pharmacology and Toxicology, 43(1):31–45, 2003.

[3] W. Rocchia, E. Alexov, and B. Honig. Extending the applicability of the nonlinear Poisson-Boltzmann equation: multiple dielectric constants and multivalent ions. The Journal of Physical Chemistry B, 105(28):6507–6514, 2001.

[4] B. Honig and A. Nicholls. Classical electrostatics in biology and chemistry. Science, 268(5214):1144–1149, 1995.

[5] G. Tresset, W.C.D. Cheong, and Y.M. Lam. Role of multivalent cations in the self-assembly of phospholipid-DNA complexes. The Journal of Physical Chemistry B, 111(51):14233–14238, 2007.

[6] G. Tresset, W.C.D. Cheong, Y.L.S. Tan, J. Boulaire, and Y.M. Lam. Phospholipid-based artificial viruses assembled by multivalent cations. Biophysical Journal, 93(2):637–644, 2007.

[7] T.S. Sorenson. Surface chemistry and electrochemistry of membranes. Taylor and Francis, CRC Press, 1999.

[8] S.A. Tatulian. Evaluation of ion binding of zwitterionic membranes based on extended Gouy-Chapman-Stern theory. The Journal of Physical Chemistry, 98(19):4963–4965, 1994.

[9] A. McLaughlin, C. Grathwohl, and S. McLaughlin. The adsorption of divalent cations to phosphatidylcholine bilayer membranes. Biochimica et Biophysica Acta (BBA)-Biomembranes, 513(3):338–357, 1978.

[10] G. Tresset. Generalized Poisson-Fermi formalism for investigating size correlation effects with multiple ions. Physical Review E, 78:061506, 2008.

[11] M. Eigen and E. Wicke. The thermodynamics of electrolytes at higher concentration. The Journal of Physical Chemistry, 58:702–714, 1954.

[12] R. Kjellander and S. Marčelja. Correlation and image charge effects in electric double layers. Chemical Physics Letters, 112:49–53, 1984.

[13] Y. Liu, M.X. Liu, W.-M. Lau, and J. Yang. Ion size and image effect on electrokinetic flows. Langmuir: the ACS Journal of Surfaces and Colloids, 24:2884–2891, 2008.

[14] C.D. Santangelo. Computing counterion densities at intermediate coupling. Physical Review E, 73(4):041512, 2006.

[15] M.Z. Bazant, B.D. Storey, and A.A. Kornyshev. Double layer in ionic liquids: Overscreening versus crowding. Physical Review Letters, 106(4):046102, 2011.

[16] B.D. Storey and M.Z. Bazant. Effects of electrostatic correlations on electrokinetic phenomena. Physical Review E, 86:056303, 2012.

[17] J.-L. Liu. Numerical methods for the Poisson-Fermi equation in electrolytes. Journal of Computational Physics, 247:88–99, 2013.

[18] D.C. Grahame. Effects of dielectric saturation upon the diffuse double layer and the free energy of hydration of ions. Journal of Chemical Physics, 18:903–909, 1950.

[19] I. Babuska. The finite element method for elliptic equations with discontinuous coefficients. Computing, 5:207–213, 1970.

[20] Z. Cai, X. Ye, and S. Zhang. Discontinuous Galerkin finite element methods for interface problems: A priori and a posteriori error estimations. SIAM Journal on Numerical Analysis, 49(5):1761–1787, 2011.

[21] R.E. Ewing, Z. Li, T. Lin, and Y. Lin. The immersed finite volume element methods for the elliptic interface problems. Mathematics and Computers in Simulation, 50(1):63–76, 1999.

[22] X. He, T. Lin, and Y. Lin. Interior penalty bilinear IFE discontinuous Galerkin methods for elliptic equations with discontinuous coefficient. Journal of Systems Science and Complexity, 23(3):467–483, 2010.

[23] R. J. LeVeque and Z. Li. The immersed interface method for elliptic equations with discontinuous coefficients and singular sources. SIAM Journal on Numerical Analysis, 31(4):1019–1044, 1994.

[24] Z. Chen and J. Zou. Finite element methods and their convergence for elliptic and parabolic interface problems. Numerische Mathematik, 79:175–202, 1998.

[25] R. Lan and P. Sun. A monolithic arbitrary Lagrangian-Eulerian finite element analysis for a Stokes/parabolic moving interface problem. Journal of Scientific Computing, 82:59, 2020.

[26] I. Kesler, R. Lan, and P. Sun. The arbitrary Lagrangian-Eulerian finite element method for a transient Stokes/parabolic interface problem. International Journal of Numerical Analysis and Modeling, 18(3):339–361, 2021.

[27] C. Wang and P. Sun. A fictitious domain method with distributed Lagrange multiplier for parabolic problems with moving interfaces. Journal of Scientific Computing, 70:686–716, 2017.

[28] A. Lundberg, P. Sun, C. Wang, and C.-S. Zhang. Distributed Lagrange multiplier/fictitious domain finite element method for a transient Stokes interface problem with jump coefficients. Computer Modeling in Engineering & Sciences, 119:35–62, 2019.

[29] R. Lan, M. J. Ramirez, and P. Sun. Finite element analysis of an arbitrary Lagrangian-Eulerian method for Stokes/parabolic moving interface problem with jump coefficients. Results in Applied Mathematics, 8:100091, 2020.

[30] W. Hao, P. Sun, J. Xu, and L. Zhang. Multiscale and monolithic arbitrary Lagrangian-Eulerian finite element method for a hemodynamic fluid-structure interaction problem involving aneurysms. Journal of Computational Physics, 433:110181, 2021.
[31] P. Sun. Fictitious domain finite element method for Stokes/elliptic interface problems with jump coefficients. Journal of Computational and Applied Mathematics, 356:81–97, 2019.
[32] R. Lan and P. Sun. A novel arbitrary Lagrangian-Eulerian finite element method for a parabolic/mixed parabolic moving interface problem. Journal of Computational and Applied Mathematics, 383:113125, 2021.
[33] P. Sun and C. Wang. Distributed Lagrange multiplier/fictitious domain finite element method for Stokes/parabolic interface problems with jump coefficients. Applied Numerical Mathematics, 152:199–220, 2020.
[34] P. Sun, C. Zhang, R. Lan, and L. Li. An advanced ALE-mixed finite element method for a cardiovascular fluid-structure interaction problem with multiple moving interfaces. Journal of Computational Science, 50:101300, 2021.
[35] M. He, P. Sun, and H. Zhao. Finite element approximations to a fourth-order modified Poisson-Fermi equation for electrostatic correlations in concentrated electrolytes. Computers and Mathematics with Applications, 117:229–244, 2022.
[36] Y.-M. Wang. On fourth-order elliptic boundary value problems with nonmonotone nonlinear function. Journal of Mathematical Analysis and Applications, 307:1–11, 2005.
[37] J.F. Traub. Iterative methods for the solution of equations. Chelsea Publishing Company, New York, 1982.
[38] Alberta Marie Harder. Fixed point theory and stability results for fixed point iteration procedures. Ph.D. thesis, University of Missouri–Rolla, Missouri, 1987.
[39] Petko D. Proinov. Unified convergence analysis for Picard iteration in n-dimensional vector spaces. Computing and Visualization in Science, 6:1–21, 2004.
[40] Ioana Timis. New stability results of Picard iteration for contractive type mappings. Fasciculi Mathematici, 56:167–184, 2016.
[41] S.C. Brenner and L.R. Scott. The mathematical theory of finite element methods. Springer, New York, 2000.
[42] Mariano Giaquinta. Introduction to regularity theory for nonlinear elliptic systems. Basel; Boston: Birkhäuser, 1993.
[43] Alain Bensoussan and Jens Frehse. Regularity results for nonlinear elliptic systems and applications. 2002.
[44] G.R. Cirmi and S. Leonardi. Regularity results for solutions of nonlinear elliptic equations with $L^{1,\lambda}$ data. Nonlinear Analysis: Theory, Methods & Applications, 69(1):230–244, 2008.
[45] Yunfeng Shi. Analytic solutions of nonlinear elliptic equations on rectangular tori. Journal of Differential Equations, 267(9):5576–5600, 2019.
[46] J. Douglas and T. Dupont. A Galerkin method for a nonlinear Dirichlet problem. Mathematics of Computation, 29(131):689–696, 1975.
[47] J. Pedro de Souza and M.Z. Bazant. Continuum theory of electrostatic correlations at charged surfaces. The Journal of Physical Chemistry C, 124(21):11414–11421, 2020.
[48] K. Besteman, M. Zevenbergen, and S.G. Lemay. Charge inversion by multivalent ions: dependence on dielectric constant and surface-charge density. Physical Review E, 72:061501, 2005.
[49] K. Besteman, M.A. Zevenbergen, H.A. Heering, and S.G. Lemay. Direct observation of charge inversion by multivalent ions as a universal electrostatic phenomenon. Physical Review Letters, 93(17):170802, 2004.

School of Sciences, Hangzhou Dianzi University, Hangzhou, Zhejiang 310018, China
E-mail: mengjieliujs@163.com

School of Sciences, Hangzhou Dianzi University, Hangzhou, Zhejiang 310018, China
E-mail, Corresponding author: hemingyan@hdu.edu.cn

Department of Mathematical Sciences, University of Nevada, Las Vegas, 4505 Maryland Parkway, Las Vegas, Nevada 89154, USA
E-mail, Corresponding author: pengtao.sun@unlv.edu